Wind Energy

WIND ENERGY
Wind Energ. 2016; **19**:1733–1747
Published online 9 November 2015 in Wiley Online Library (wileyonlinelibrary.com). DOI: 10.1002/we.1940

PAPER PRESENTED AT AWEA WINDPOWER

Vibration-based wind turbine planetary gearbox fault diagnosis using spectral averaging

Jae Yoon[1], David He[1], Brandon Van Hecke[1], Thomas J. Nostrand[2], Junda Zhu[2] and Eric Bechhoefer[3]

[1] Department of Mechanical and Industrial Engineering, University of Illinois at Chicago, Chicago, Illinois 60607, USA
[2] Renewable NRG Systems, 110 Riggs Road, Hinesburg, Vermont 05461, USA
[3] Green Power Monitoring Systems, Essex Junction, Vermont 05452, USA

ABSTRACT

Planetary gearboxes (PGBs) are widely used in the drivetrain of wind turbines. Any PGB failure could lead to a significant breakdown or major loss of a wind turbine. Therefore, PGB fault diagnosis is very important for reducing the downtime and maintenance cost and improving the safety, reliability, and lifespan of wind turbines. The wind energy industry currently utilizes vibratory analysis as a standard method for PGB condition monitoring and fault diagnosis. Among them, the vibration separation is considered as one of the well-established vibratory analysis techniques. However, the drawbacks of the vibration separation technique as reported in the literature include the following: potential sun gear fault diagnosis limitation, multiple sensors and large data requirement, and vulnerability to external noise. This paper presents a new method using a single vibration sensor for PGB fault diagnosis using spectral averaging. It combines the techniques of enveloping, Welch's spectral averaging, and data mining-based fault classifiers. Using the presented approach, vibration fault features for wind turbine PGB are extracted as condition indicators for fault diagnosis and condition indicators are used as inputs to fault classifiers for PGB fault diagnosis. The method is validated on a set of seeded localized faults on all gears: sun gear, planetary gear, and ring gear. The results have shown a promising PGB fault diagnosis performance with the presented method. Copyright © 2015 John Wiley & Sons, Ltd.

KEYWORDS

planetary gearbox; fault diagnosis; vibration; spectral averaging; condition monitoring; condition indicator

Correspondence

D. He, Department of Mechanical and Industrial Engineering, University of Illinois at Chicago, Chicago, Illinois 60607, USA.
E-mail: davidhe@uic.edu

Received 21 May 2015; Revised 2 August 2015; Accepted 21 September 2015

1. INTRODUCTION

Wind energy is one of the fastest growing energy sources among various renewable energy options. Establishment of more proactive maintenance strategy is needed before the recently deployed massive industrial wind projects enter the wear-out failure zone. This is more important for the off-shore wind farms, where not only the availability of the site for maintenance can be restricted but also the saline environment easily accelerates the mechanical and chemical failures.

Planetary gearboxes (PGBs) are commonly used in the design of wind turbine drivetrain systems as their unique design allows distributing the input torque in parallel and minimizing gearbox size. As reported in Sheng *et al.*,[1] the gearbox failure is the first leading contributor (~22%) to total wind turbine downtime. It was also shown in Sheng[2] that the gear failure accounted for 26 and 25% of all gearbox failures observed in 2013 and 2014, respectively. Therefore, PGB fault diagnosis is an important aspect in reducing the downtime and maintenance cost and improving the reliability and lifespan of wind turbines.

In general, vibration behavior is the most widely researched machine condition parameter in the field of machinery fault diagnostics (e.g. bearings, gears, and shafts). Time synchronous averaging (TSA) is a popular signal processing technique for vibration analysis used to extract a periodic waveform from noisy signals of rotating machines (Braun[3] and McFadden[4]). The underlying idea of TSA is to intensify a periodically repeated waveform by computing the

ensemble average of successive periods of a waveform of interest. Although TSA has been widely accepted to gear applications with fixed axes, literature to date barely finds TSA-based PGB fault diagnosis. As reported in the literature, PGB fault diagnosis is complicated for the following two reasons: (i) the complexity in dynamic rolling structures does not allow for direct attachment of sensors within the rotating elements, for example, the sun and planet gears (Samuel *et al.*[5]) and (ii) PGB includes multiple gear meshes and other parameters such as planet phasing and load sharing. Gear manufacturing errors can introduce complicated gear mesh excitations (Luo *et al.*[6]). Because of the structural complicacy of PGB, the 'amplitude modulation (AM) effect' is observed in vibration analysis. Provided in Figure 1, an example of AM effect is displayed. A modified version of the TSA, vibration separation (VS) introduced by McFadden and Howard[7] and Howard[8] was improved as follows: McFadden[9] introduced the use of other window functions such as triangular and Hanning, rather than rectangular window in the original VS framework, Samuel *et al.*[5] applied the constrained adaptive lifting algorithm to enhance the detection of local wave-form changes caused by gear damage types, and Lewiki *et al.*[10] used the method in McFadden[9] to provide a comprehensive diagnostics for helicopter transmission including gear and bearing. The applicability of the VS was extended to fiber optic strain signal analysis by Kiddy *et al.*[11] The underlying idea of VS technique is to decompose a raw vibration signal into individual PGB component (e.g. sun gear or planet gears) oriented vibration signals. First, windowed vibration signals are taken when the vibration sensor, ring gear, planet gear, and sun gear are aligned radially inline. Assuming that each planet gear and sun gear have k and l numbers of teeth respectively, k and l windowed vibration signals are taken for planet gear VS and sun gear VS. These windowed vibration signals are then rearranged and stitched by utilizing the PGB geometric properties such as the gear teeth orders for the targeting gear component. The drawbacks of the VS technique summarized in Samuel *et al.*[5] include the following: (i) under specific PGB geometries, VS cannot capture sun gear data; (ii) sufficiently large recording time is required to obtain the final set; and (iii) VS is vulnerable to external noises.

Other vibration-based approaches have been reported in the literature. Yang *et al.*[12] discussed practical wind turbine condition monitoring challenges with the currently available condition monitoring techniques. Siegel *et al.*[13] provided a comparative study over the established vibratory analysis methods for wind turbine condition monitoring. The compared vibratory analysis methods include the following: frequency domain, cepstrum, enveloping, spectral kurtosis filtering, TSA, and VS methods. Luo *et al.*[14] introduced a digital domain synchronous sampling and order analysis approach to detect bearing and gear damage features under wind turbine nonstationary operational conditions. Sawalhi *et al.*[15] presented a wind turbine condition monitoring technique over four separate stages. Bearing diagnosis was carried out using a

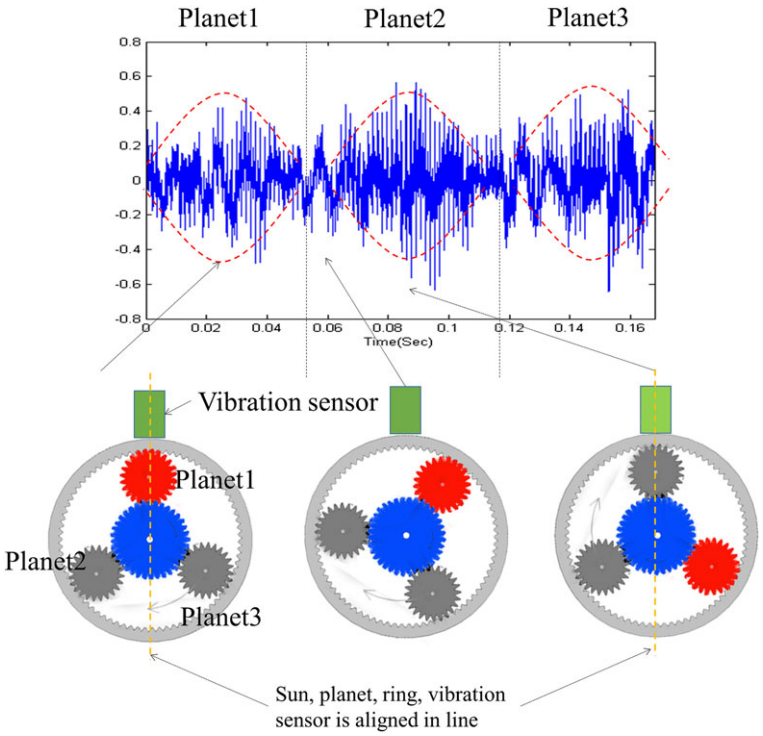

Figure 1. The AM effect of vibration signal on PGB.

Wind Energ. 2016; **19**:1733–1747 © 2015 John Wiley & Sons, Ltd.
DOI: 10.1002/we

combination of whitening the residual signal, kurtogram, and Hilbert transform approach to get the spectrum of the squared envelope. Gear diagnosis was carried out using spectrum and cepstrum analysis and VS technique. Wang *et al.*[16] proposed a wind turbine fault detection method without requiring a priori information such as rotating speeds. Their method includes ensemble empirical mode decomposition followed by independent component analysis. Wu *et al.*[17] showed the detectability of cracks on a PGB planet carrier. In their study, raw vibration and TSA data were transferred to the frequency domain and wavelet domain to extract the fault features. Patrick *et al.*[18] presented a vibration-based on-board fault diagnosis and failure prognosis for helicopter transmissions. In their study, TSA was used for pre-processing vibration data and a particle filter was used for fault diagnosis and failure prognosis. Bartelmus and Zimroz[19] showed that the vibration spectral characteristics of a PGB can be used for fault detection and location. Barszcz and Randall[20] applied the spectral kurtosis method for PGB fault detection of gear tooth cracks in wind turbine applications. Feng and Zuo[21] derived mathematical models of PGB for detecting and locating faults by considering characteristic frequencies of AM and frequency modulation (FM) effects. However, none of the reported method has presented a vibratory analysis which effectively differentiates varied localized faults on all gears: sun gear, planetary gear, and ring gear.

In this paper, a new method using a single vibration sensor for PGB fault diagnosis will be presented. The method combines the techniques of enveloping and Welch's spectral averaging (SA). Spectral averaging for bearing fault diagnosis has been recently reported in Bechhoefer *et al.*[22] and Van Hecke *et al.*.[23] Using the presented approach, vibration fault features for wind turbine PGB are extracted as condition indicators (CIs) for fault diagnosis. The method is validated on a set of seeded localized faults on all gears: sun gear, planetary gear, and ring gear. The remainder of the paper is organized as follows. Section 2 gives a detailed explanation of the proposed methodology. In Section 3, the details of the seeded fault tests on a laboratory PGB test rig and the experimental setup used to validate the proposed methodology are provided. Section 4 presents the PGB fault diagnostic results from the seeded fault tests. Finally, Section 5 concludes the paper.

2. METHODOLOGY

The framework of the methodology for wind turbine PGB fault diagnosis is provided in Figure 2. The methodology will be explained in three sections. Section 2.1 discusses the SA-based approach for processing the PGB vibration signals followed by computation of CIs in Section 2.2. Section 2.3 explains the data mining approaches for fault diagnosis using the CIs as inputs.

2.1. Spectral averaging based machinery fault diagnosis

First, the original Welch's power spectral density (PSD) estimate is introduced. Welch[24] expressed the theoretical background of SA by letting $X(j)$, for $j = 0, \ldots, N-1$ be a sample from a stationary, stochastic sequence with expected value of $E(X(j)) = 0$ and letting $X(j)$ have spectral density $P(f)$, $|f| \leq \frac{1}{2}$, where f is the normalized frequency. Note that N refers to

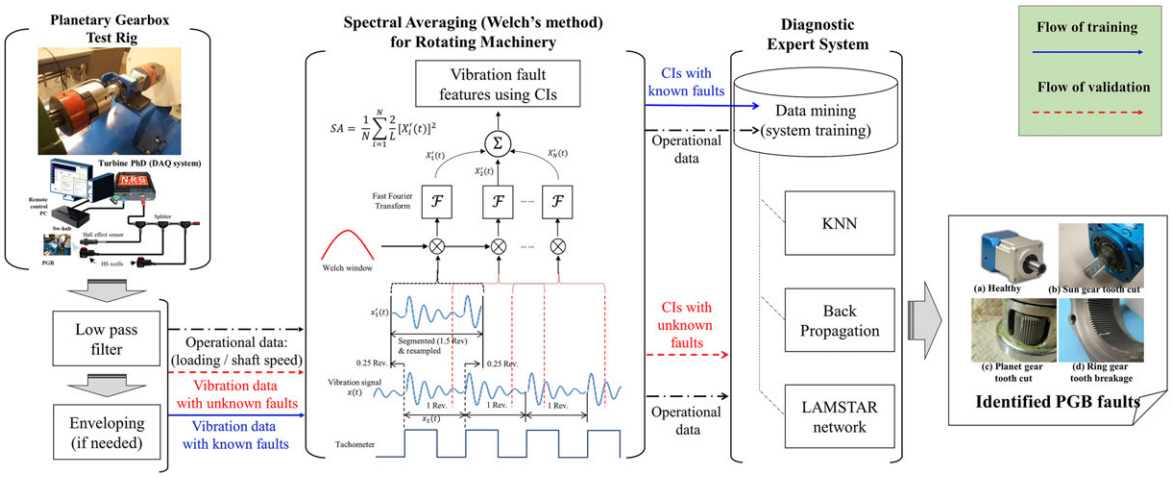

Figure 2. The framework of the methodology for PGB fault diagnosis.

the total number of samples from the process $X(j)$. Then if one takes several possibly overlapping segments of length L with starting points of the segments M units apart and letting $X_1(j), j = 0, \ldots, L-1$ be the first segment. Then,

$$X_1(j) = X(j), \quad \text{for } j = 1, \ldots, L-1 \tag{1}$$

Likewise,

$$X_2(j) = X(j+M), \quad \text{for } j = 1, \ldots, L-1 \tag{2}$$

And, finally,

$$\mathrm{X}_k(j) = X(j+(K-1)M), \quad \text{for } j = 1, \ldots, L-1 \tag{3}$$

The result comprises K segments $X_1(j), \ldots, X_k(j)$ covering the entire sample of interest such that $(K-1)M+L=N$. Then, from each modified segment of length L, a periodogram is obtained. In other words, a proper windowing function can be applied before Fourier transforms is applied to each segment. This can be expressed in mathematical form as

$$F_k(n) = \frac{1}{L}\sum_{j=0}^{L-1} X_k(j) W(k) e^{-i(2kjn/L)} \tag{4}$$

where i stands for the imaginary unit. The periodograms correspond to the K number of segments and can be obtained as

$$B_k(f_n) = \frac{L}{S}|F_k(n)|^2, \quad \text{for } k = 1, 2, \ldots, K \tag{5}$$

where $f_n = \frac{n}{L}$, for $\mathrm{n} = 0, \ldots, \frac{L}{2}$; $\mathrm{S} = \frac{1}{L}\sum_{j=0}^{L-1} W^2(j)$. Finally, the Welch's PSD estimate, $\hat{P}(f_n)$, is obtained by averaging equation (5) as

$$\hat{P}(f_n) = \frac{1}{K}\sum_{k=1}^{K} B_k(f_n) \tag{6}$$

Next, the implementation of Welch's SA is explained. Figure 3 displays a graphical representation of the SA for rotating machinery fault diagnosis shown in Van Hecke *et al.*.[23] To implement the SA for machinery fault diagnosis, the sensor signals must be segmented by a particular size. According to the original research of Welch's SA method,[24] it is suggested to have a 50% overlap (e.g. 25% overlap front and back) for each windowed signal. The shaft revolutionary information is first obtained by using the zero-crossing counts of the tachometer signals. The data points in each revolution is interpolated and resampled into equally sized revolutions by applying the time synchronized resampling (TSR). It has been shown that by using TSR, potential fluctuations in shaft speed can be accounted for, and the effect of spectral smearing reduced (Bechhoefer *et al.*[22]). The resampling is achieved by interpolating the original data points in one shaft revolution into the next radix 2 such that each revolution contains an equal number of data points for the TSR. Then the two 25% overlaps were attached to front and back of the TSR performed data points (e.g. segmented or rectangular windowed) before and after to apply SA. Note that in this case, the number of resampled data points L is equal to the length of the segments. The SA-based vibration fault features can be obtained from the time domain signal as

$$x_{SA} = \mathrm{real}\left(\mathcal{F}^{-1}\left(|\mathcal{F}(x)|^2\right)\right) \tag{7}$$

where real (•) returns real value of (•), $\mathcal{F}$ and $\mathcal{F}^{-1}$ represent Fourier transform and inverse Fourier transform, respectively. $|\mathcal{F}(x)|^2$ originally refers to PSD of the signal x but is replaced with the PSD estimate using Welch's method in this paper. The term 'Welch' indicates the CIs computed from x_{SA}, hereafter.

2.2. Condition indicators

In this paper, the CIs reported effective in Sheng[25] for gear fault diagnosis using vibration signals for wind turbine applications will be computed. These CIs can be grouped into five types: root mean square (*RMS*), peak to peak (*P2P*), skewness (*SK*), kurtosis (*KT*), and crest factor (*CF*). Each type of CI can be computed using different input signals. In addition to raw vibration signals, other types of input signals will be generated by pre-processing the raw vibration signals as residual, energy operator (EO), narrow band (NB), AM, and FM, A residual signal is a time domain signal with the primary meshing

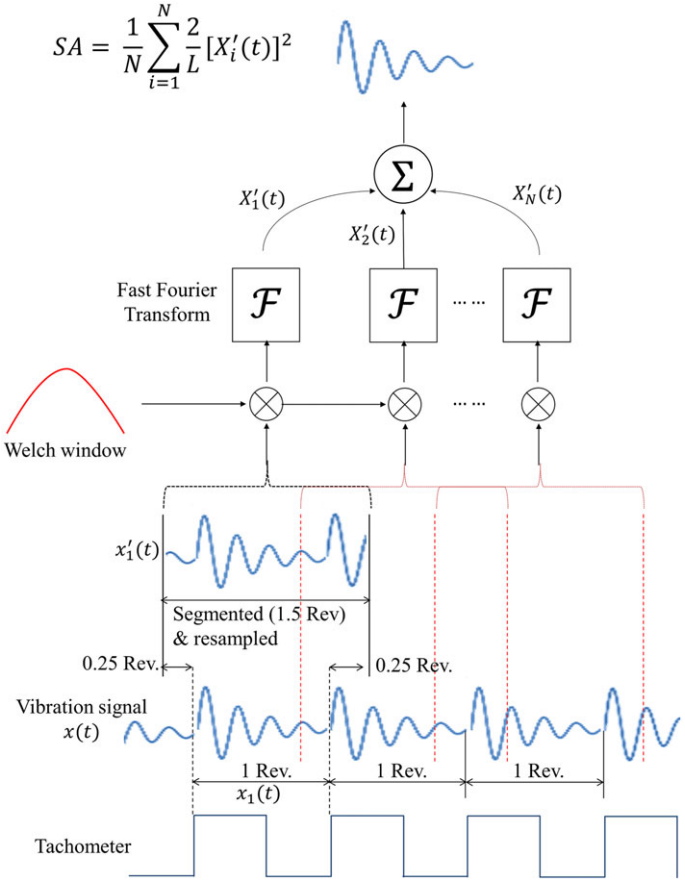

Figure 3. Welch's method for machinery fault diagnosis.

and shaft components removed from the input signal. Gear distributed fault (GDF) is used as an effective CI for distributed gear faults wear and multiple tooth cracks. GDF[26] is calculated from the formula in the succeeding texts:

$$GDF = \frac{\text{StdDev(residual signal)}}{\text{StdDev(original signal)}} \tag{8}$$

The EO introduced by Teager[27] represents the 'total energy', both kinetic energy (KE) and potential energy (PE), of a signal of interest. Although this is strictly only true for a displacement signal, where the square of the velocity (i.e. derivative of the displacement) is proportional to the KE, and the square of the Hilbert transform of the velocity (90° out-of-phase) is proportional to the PE (with the same proportionality constant). Thus, in general, the EO is equal to the squared envelope of the derivative of a signal. It certainly seems to make sense to use the EO for synchronously averaged gear signals, because taking the derivative would put more weight on the higher harmonics of gear meshing frequency and emphasize impulsiveness. The EO is defined as

$$x_{EO,i} = x_{IN,i}^2 - x_{IN,\,i-1} \cdot x_{IN,i+1}, \quad (\text{for } i = 2,\ 3,\ \ldots,\ L-1) \tag{9}$$

where $x_{EO,i}$ is the ith element of EO data and $x_{IN,i}$ is the ith element of the input data x_{IN}. In this paper, the NB analysis was performed to capture sideband modulation of the gear mesh tones to detect the cracked or broken tooth. The NB filtered signal, x_{NB}, could be obtained by filtering out all tones except those of the gear mesh and the characteristic frequencies. The characteristic frequencies refer to the sun gear fault frequency, planet gear fault frequency, and ring gear fault frequency, respectively. Also, the passband of the NB filter was set to the frequency of interest ± 2 Hz. AM and FM CIs are obtained by AM analysis and FM analysis of x_{NB}. AM and FM signals are absolute value and the derivative of the angle of the analytic signal formed by adding i times the Hilbert transform of x_{NB} to x_{NB}, respectively. For more details of NB, AM, and FM, please see Sheng.[25] Finally, Welch's method is further processed to obtain Welch CIs and Welch EO CIs. Table I provides the definitions of the CIs investigated for PGB fault diagnosis in this paper.

Table I. The definitions of the CIs.

		Input signal (x_{IN})						
		Raw	EO	NB	AM	FM	Welch	Welch EO
Basis CI	Formula	Time synchronous averaged and raw signal (x_{TSA}/x_{raw})	A residual of the autocorrelation function (x_{EO})	Narrow band pass filtered (x_{NB})	Amplitude modulation of NB filtered signal [$AM(x_{NB})$]	Frequency modulation of NB filtered signal [$FM(x_{NB})$]	Welch windowed spectral averaging (x_{SA})	Energy operator of Welch [$(x_{SA})_{EO}$]
Root mean square (*RMS*)	$RMS(x_{IN}) = \sqrt{\frac{1}{L}\sum_{i=1}^{L} x_i^2}$	$RMS(x_{IN})$: measurement computes root mean square from the input data in a scalar form. In a strict mathematical term, this function performs a sample standard deviation if the direct current is removed.						
Peak to peak (*P2P*)	$P2P(x_{IN}) = \frac{[\max_{1\le i\le L}(x_i) - \min_{1\le i\le L}(x_i)]}{2}$	$P2P(x_{IN})$: measures the maximum difference within the input signal.						
Skewness (*SK*)	$SK(x_{IN}) = \frac{\frac{1}{L}\sum_{i=1}^{L}(x_i-\bar{x})^3}{\left[\sqrt{\frac{1}{L}\sum_{i=1}^{L}(x_i-\bar{x})^2}\right]^3}$	$SK(x_{IN})$: measures the asymmetry of the input signal about its mean value. A negative *SK* value and a positive *SK* value imply that the data have a longer or fatter left tail and the data have a longer or fatter right tail, respectively.						
Kurtosis (*KT*)	$KT(x_{IN}) = \frac{L\sum_{i=1}^{L}(x_i-\bar{x})^4}{\left[\sum_{i=1}^{L}(x_i-\bar{x})^2\right]^2}$	$KT(x_{IN})$: measures the peakedness, smoothness, and the heaviness of tail in the input signal.						
Crest factor (*CF*)	$CF(x_{IN}) = \frac{P2P(x_{IN})}{RMS(x_{IN})}$	$CF(x_{IN})$: measures the ratio between $P2P(x_{IN})$ and $RMS(x_{IN})$ to describe how extreme the peaks are in the input signal.						

Note: x_i is ith element of the input data x_{IN}; L is the length of the input data x_{IN}; max(·) returns the maximal element of input data x_{IN}; min(·) returns the minimal element of input data x_{IN}; $\bar{x}$ is a mean value of the input data x_{IN} defined as $\sum_{i=1}^{L} x_i/L$; and NB, AM, and FM refers to a narrow band, amplitude modulation, and frequency modulation, respectively.

DOI: 10.1002/we

2.3. Data mining-based fault diagnosis

Three supervised learning algorithms are used to construct the PGB fault classifier: *k*-nearest neighbor (KNN), back propagation (BP), and large memory storage and retrieval (LAMSTAR).

2.3.1. *K*-nearest neighbor

KNN (Altman[28]) is one of the most popular choices for fault classifiers. KNN has been reported as an effective fault classifier for bearing fault diagnosis (He *et al.*[29]). KNN assumes the data set as points in a *p*-dimensional space where *p* is the number of CIs. A fault is classified by taking the majority vote of its neighbors; voting is nothing but identifying the *k* number of nearest observations in the training data set and their associated fault classes from the Euclidean or Hamming distance perspectives. In general, a larger value of *k* is preferred for suppressing the noise effect, while the good *k* selecting procedure varies by data set and it is mostly heuristic. A shortcoming of the KNN is that it is sensitive to the local structure of the data. Meanwhile, the implementation is straightforward in comparison to other popular machine learning techniques.

2.3.2. Back propagation

Artificial neural network (ANN) is a computational model that mimics the biological central nervous system such as human or animals. It consists of simple processing elements (also called as neurons) connected in a complex layered structure which enables the model to simulate a complex non-linear function. BP network (Rumelhart *et al.*[30]) is the most representing ANN methodology, which performs weight adjustment back and forth using gradient descent. The decision-making principles in the most of ANN approaches are similar. If the '*n*' inputs denoted as $\{x_{ij}; i = 1, 2, \ldots, n\}$ are fed into *j*th neuron, output 'y_j' satisfies as

$$y_j = \mathrm{f_n}\left[\sum_{i=1}^{n} w_{ij} x_{ij}\right] \tag{10}$$

where $\mathrm{f_N}(\cdot)$ represents nonlinear activation function. A couple of known drawbacks for BP network are as follows: (i) it could potentially be captured by a local minima and (ii) the convergence of BP learning is slow.

2.3.3. LAMSTAR network

While LAMSTAR network (Graupe and Kordylewski[31]) is a powerful fault classifier, LAMSTAR has barely been reported in the literature for machinery fault detection and diagnosis. However, LAMSTAR network has been reported from biomedical, financial, and image processing fields because of its rapid processing capability. Previously LAMSTAR network was US patented but its patent protection currently has expired according to the Google's patent search engine (Google Patent[32]). LAMSTAR network is Kohonen's self-organizing map (Kohonen[33]) based ANN, which claims to be less sensitive to local minima and faster in training than BP and support vector machine (Graupe[34]). Its unique link-weight system attempts to imitate the efficient storage and retrieval capabilities in big data applications. In addition, its inherent transparency provided by the link-weight structure enables the application of forgetting to time-varying problems. In reference Kordylewski *et al.*,[35] LAMSTAR network was shown to be almost 1000 times faster than BP network while a similar level of classification accuracy was achieved. The implementation details of LAMSTAR can be found in Graupe.[34]

3. EXPERIMENTAL SETUP

This section covers the experimental setup used to validate the presented PGB fault diagnostic method. First, the PGB test rig and the characteristic frequencies of the PGB associated with the test rig are briefly introduced in Section 3.1. Then, the seeded gear fault test procedure and data acquisition (DAQ) plan will be shown in Section 3.2.

3.1. The planetary gearbox test Rig.

Figure 4 displays the PGB test rig in the laboratory. It composes four main parts: (i) the DAQ system, (ii) the driving part, (iii) the PGB gearbox, and (iv) the load generator. The DAQ system includes a local data collector (model: turbine PhD by renewable NRG systems), two high-speed accelerometers, and tachometer. A Hall effect sensor and a toothed wheel mounted on the motor shaft were paired to record the real-time shaft rotating remarks. The detail DAQ settings are provided in Table II. The driving motor is a three-phase 10 HP induction motor with a motor controller. The output shaft of the gearbox is connected to a generator and a grid tie which serves as a load generator. The structure of the PGB test rig is similar to those used in a wind turbine. During the test, commercially available single-stage PGBs with a 5:1 speed reduction ratio were used.

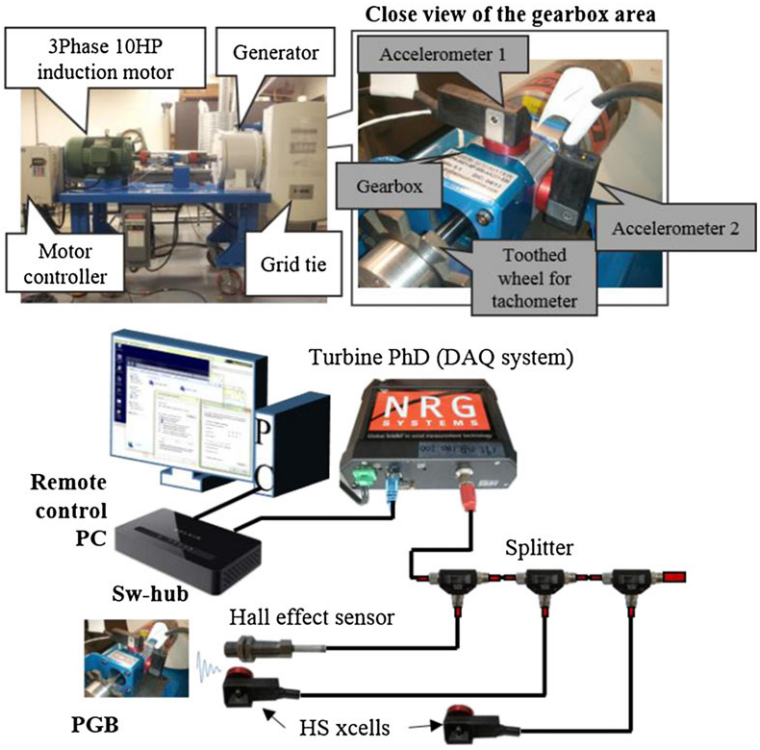

Figure 4. The PGB test rig for wind turbine simulator.

Table II. Vibration DAQ settings.

	Vibration sensor 1	Vibration sensor 2	Tachometer
Sensor	High-speed accelerometer	High-speed accelerometer	Hall effect sensor
Manufacturer	NRG systems	NRG systems	Sensoronix
Sampling rate	6104 (Hz)	24 414 (Hz)	1000 (Hz)
Sample recoding time for TSA	40 (s) × 5 samples	20 (s) × 5 samples	—
Sample recording time for SA	4 (s) × 50 samples	2 (s) × 50 samples	—

Amongst the three different PGB operational types, a specific PGB with the fixed ring gear was used in this paper. Figure 5 shows a notional sketch of the PGB structure with the fixed ring gear. For this type of PGB, the number of teeth is linear to the radius of each gears pitch circle. This indicates that the input to output velocity ratio is also related to the angular velocity (ω) of the gears. The gear ratio can be defined as

$$\begin{aligned} R &= \frac{\omega_{sun}}{\omega_{carrier}} \\ &= 1 + \frac{z_{ring}}{z_{sun}} \end{aligned} \tag{11}$$

where ω_i is the angular velocities on gear component i and z_j is the number of teeth on gear component j;

The planet carrier rotation speed (i.e. output speed) in frequency could be obtained as

$$f_{carrier} = \frac{f_{sun}}{R} \tag{12}$$

where f_i is the rotation speed in frequency at gear component i. Also, a meshing characteristic frequency of PGB can be obtained as

$$f_{sun/planet} = f_{planet/ring} = \frac{f_{sun} z_{sun} z_{ring}}{(z_{sun} + z_{ring})} = \frac{f_{sun} \cdot z_{ring}}{R} \tag{13}$$

Wind Energ. 2016; **19**:1733–1747 © 2015 John Wiley & Sons, Ltd.
DOI: 10.1002/we

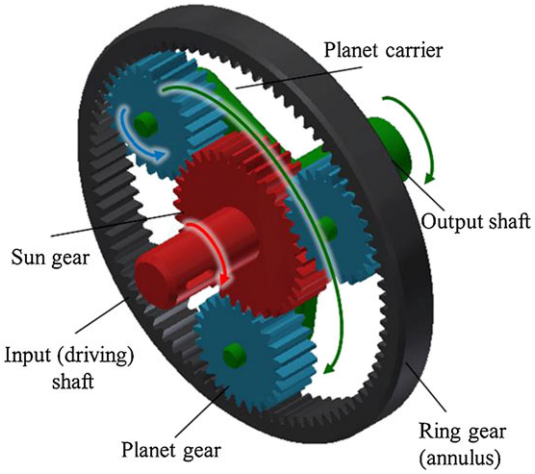

Figure 5. Notional sketch of a PGB structure.

where f_{ij} is the relative rotation speed in frequency between gear components i and j. The most common three failure modes of the PGB are the sun gear fault, planet gear fault, and ring gear fault. The corresponding fault frequencies are represented as follows:

$$f_{f,sun} = s\cdot(f_{sun} - f_{carrier}) = \frac{f_{sun} z_{ring} s}{(z_{sun} + z_{ring})} \tag{14}$$

$$f_{f,planet} = 2\left(f_{planet} + f_{carrier}\right) = \frac{4 n_{sun} z_{sun} z_{ring}}{\left(z_{ring}^2 - z_{sun}^2\right)} \tag{15}$$

$$f_{f,ring} = s\cdot f_{carrier} = \frac{f_{sun} z_{sun} s}{(z_{sun} + z_{ring})} \tag{16}$$

where $f_{f,i}$ indicates the fault frequency at gear component i and s represents the number of planet gears in the gearbox. For more details, see Bartelmus and Zimroz.[36] Tables III and IV present the structural information and characteristic frequencies of the PGB used in this paper.

Table III. The parameters of the PGB.

Parameter	Number of teeth on sun gear (z_1)	Number of teeth on planet gear (z_2)	Number of teeth on ring gear (z_3)	Number of planet gears (s)
Value	27	41	108	3

Table IV. Characteristic frequencies of the PGB at varied input shaft speed.[a]

Input shaft speed in frequency (f_1)	Output shaft speed in frequency (f_a)	Meshing frequency ($f_{12} = f_{23}$)	Sun fault frequency ($f_{f,1}$)	Planet fault frequency ($f_{f,2}$)	Ring fault frequency ($f_{f,3}$)
10	2	216	24	10.67	6
20	4	432	48	21.33	12
30	6	648	72	32	18
40	8	864	96	42.67	24
50	10	1080	120	53.33	30

[a]All the values are in unit of hertz.

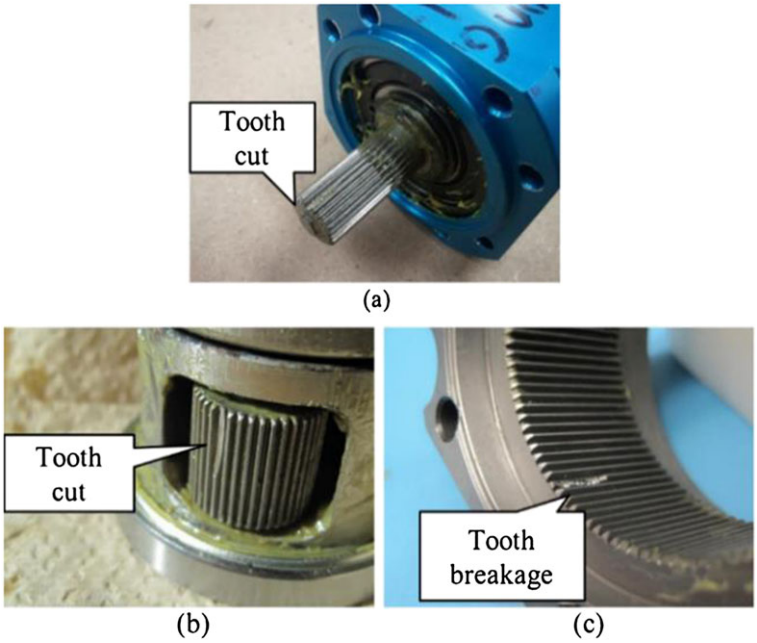

Figure 6. Seeded faults: (a) sun gear fault, (b) planet gear fault, and (c) ring gear fault.

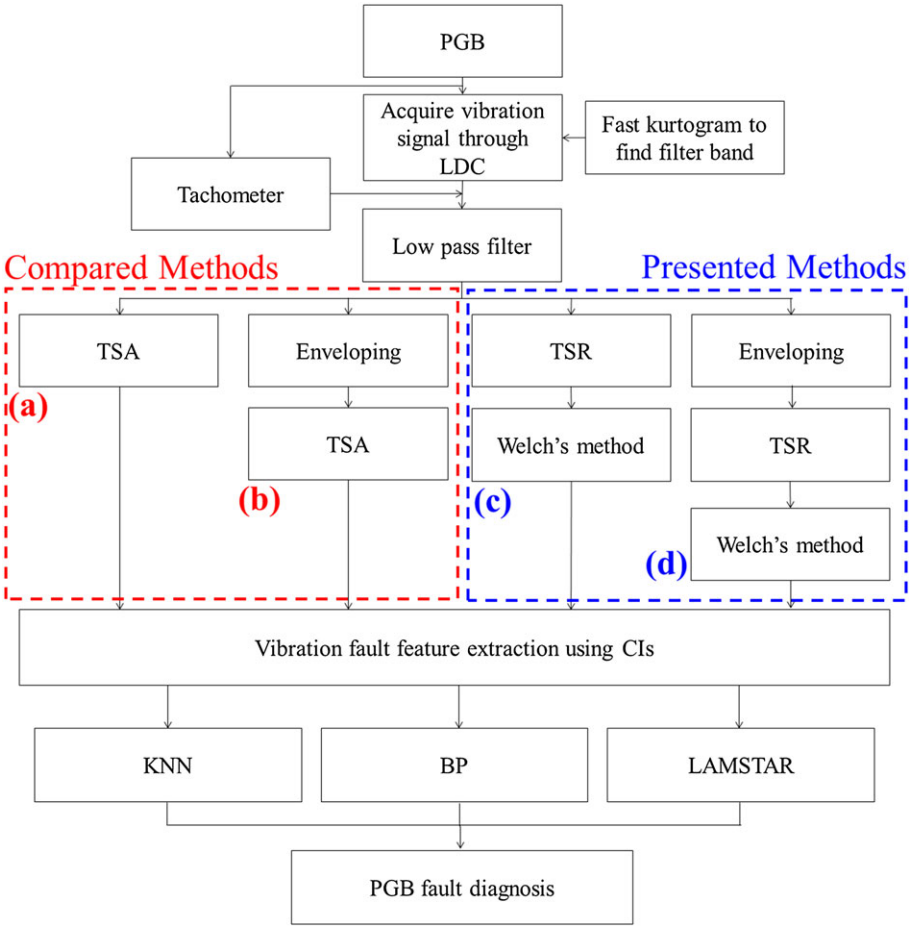

Figure 7. Overview of the experiment procedure for PGB fault diagnosis.

Wind Energ. 2016; **19**:1733–1747 © 2015 John Wiley & Sons, Ltd.
DOI: 10.1002/we

3.2. Seeded gear faults

Three types of PGB faults were created: sun gear partial tooth cut, planet gear partial tooth cut, and ring gear tooth breakage. Each type of gear fault was artificially created by damaging a tooth on a sun gear, planet gear, and ring gear as shown in Figure 6. Both healthy and faulty gearboxes were tested under 20 combinational conditions of four varying loading conditions: 0% loading, 25% loading, 50% loading, and 75% loading out of the rated torque of the PGB, and five varying shaft speeds: 10, 20, 30, 40, and 50 Hz. Vibration data were collected from each fault seeded gearbox sequentially. After switching one gearbox to another, the vibration sensors were mounted in the same location on the PGB to preserve the experimental consistency.

4. VALIDATION RESULTS

Figure 7 provides an overview of the experimental procedure that was used to generate the validation results.

As shown in Figure 7, during the experiment, vibration data were processed with two groups of methods: the presented methods and the methods to be compared with. The methods to be compared with include (a) TSA and (b) enveloping then TSA. The presented methods are the proposed solution in this paper and include (c) Welch's method (i.e. SA), (d) enveloping, TSR, and then Welch's method. After each processing technique was applied, the CIs were computed. First, low-pass filtering was performed before each vibration processing technique as shown in Figure 7. Fast kurtogram, as reported in Antoni,[37] was applied to find universal filter bands for each vibration sensor. Statistics of the impulsivity locations over varied input shaft speed suggests that the accelerometers 1 and 2 have impulsivity located below 3 and 12 kHz; thus, 3 and 12 kHz were chosen for the cutoff frequencies in the low-pass filters for accelerometers 1 and 2, respectively.

Table V gives a summary on the percentage separation of faulty gears from the healthy one using CIs generated by each of the four methods. The percentage separation is defined as the percentage of the data samples that show a statistically significant difference between the CIs of the fault gear and healthy gear. From Table V, it can be noted that the conventional signal processing techniques, methods (a) and (b), showed relatively less percentage separation than methods (c) and (d). On the other hand, the proposed method (c) and method (d) generated multiple CIs displaying PGB fault isolating performance. Also, from Table V, one can see that the most effective CIs were obtained when vibration signals of accelerometer 2 were processed with method (c). These CIs include FM0 achieving 90% separation for the sun gear fault, Res RMS and WEO RMS achieving 100% separation for the planet gear fault, and GDF achieving 100% for the ring gear fault. Figures 8 graphically shows the separation of the fault gear from the healthy gear achieved by previously mentioned CIs. Each point and the vertical bar at each point in Figure 8 represent the averaged CI value and the 95% confidence interval.

Table V. Percentage separation of the PGB faults achieved by the CIs.

		Accelerometer 1 (fs = 6104 Hz)		
		Sun fault	Planet fault	Ring fault
Method	(a) TSA	—	≥8: P2P	—
	(b) Env-TSA	—	≥8: P2P	≥8: RMS, P2P
	(c) Welch	≥8: Res RMS, Res P2P, WEO P2P	≥90%: RMS, Res RMS ≥8: P2P, Res P2P, EO P2P, W RMS, WEO P2P	≥8: Res RMS, Res CF, EO P2P, W RMS, W KRT, WEO RMS
	(d) Env-Welch	≥8: Res RMS, EO RMS, WEO P2P	≥8: P2P, Res RMS, EO RMS, EO P2P, W P2P, WEO P2P	≥8: Res RMS, EO RMS, WEO RMS, WEO P2P
		Accelerometer 2 (fs = 24414 Hz)		
		Sun fault	Planet fault	Ring fault
Method	(a) TSA	≥8: Res RMS, Res P2P, GDF	—	≥9: GDF
	(b) Env-TSA	≥8: Res RMS, Res P2P, GDF	≥8: RMS, Res RMS, Res P2P	—
	(c) Welch	≥90%: FM0 ≥8: Res RMS, Res KT, GDF	≥1%: Res RMS, WEO RMS ≥9: P2P, Res P2P, EO RMS, EO P2P, W P2P, WEO P2P ≥8: RMS, W KT, W SK	≥1%: GDF ≥9: FM0, W RMS, WEO KT, WEO SK ≥8: W KT, W CF, W SK, WEO RMS
	(d) Env-Welch	≥8: Res RMS, EO RMS, WEO P2P	≥8: P2P, Res RMS, EO RMS, EO P2P, W P2P, WEO P2P	≥8: Res RMS, EO RMS, WEO RMS, WEO P2P

Note: 'Res' stands for the residual signal and fs for the sampling frequency.

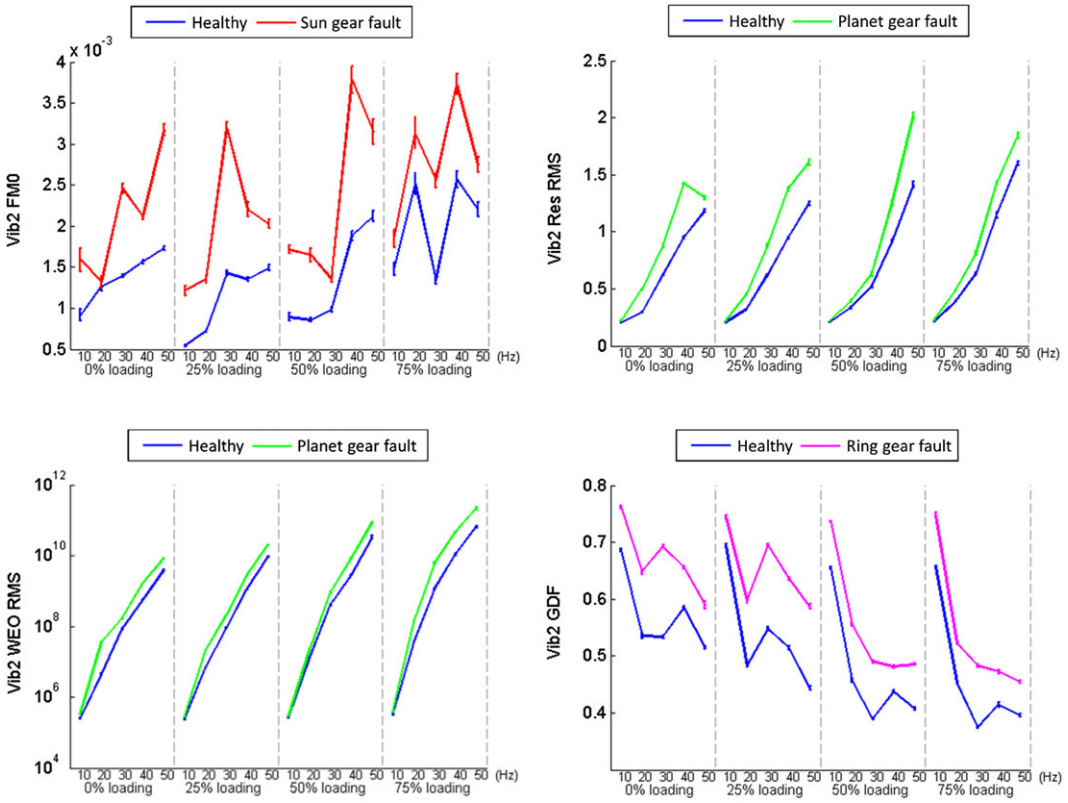

Figure 8. Effective CIs (a) FM0: healthy versus sun gear fault, (b) residual RMS: healthy versus planet gear fault, (c) WEO RMS: healthy versus planet gear fault, and (d) GDF: healthy versus ring gear fault.

Effective CIs in Table V were further utilized to diagnose the faults (e.g. sun, planet, ring, or healthy) using three fault classifiers: KNN, BP, and LAMSTAR. Tables VI and VII provide the PGB fault diagnostic results achieved by the fault classifiers with the individual CIs and combinations of CIs, respectively. PGB operational parameters such as loading condition and shaft speed were included. Out of 2000 samples, 70% of the data points were randomly chosen and utilized for training and the remaining 30% of data points were used for validation. In order to measure the statistical fault diagnostic performance, all classifiers were run 50 times in a random sampling manner. The average error rates (% of error) and its standard deviation were computed. The error rate is defined as the percentage of misclassified samples in validation. For KNN, the search radius of k was investigated within $k = 3 \sim 15$ range and the minimal error rate is shown on each table. Also, for the BP network, the neuronal structures in the hidden layer were investigated for $N = 10$, 20, 30, 40, and 50, and the one showing the minimal error is provided.

As one can see from Table VI, none of the single CIs provides acceptable diagnostic performance for all three fault classifiers although each CI can detect faults from at least one or more PGB fault types. Thus, two combinations of CIs were generated. In the first CI combination, the CIs showing the highest percentage separation in Table V (i.e. ≥90% for sun gear fault, 100% for planet gear and ring gear faults) were grouped. In the second CI combination, the CIs with the second highest percentage separation in Table V (i.e. ≥80% for sun gear fault, ≥90% for planet gear and ring gear faults) were included to the second CI combination.

The fault diagnostic results with both CIs combinations are provided in Table VII. KNN achieved the overall best error rate of 3.63% when the first CI combination was used. When the local minima convergence is ignored, BP network achieved less than an overall diagnostic error rate of 5%. However, the final error rate drastically worsened when the local minima convergence is considered. It should be noted that the occurrence of local minima convergence was approximately 12 ~ 16% over 50 runs and it is well reflected on the standard deviation of the error rate. Lastly, LAMSTAR network achieved an overall diagnostic error rate of 3.98% as it is claimed to be insensitive to the local minima issue normally associated with the BP network. However, among the three classifiers, LAMSTAR network resulted in the minimal standard deviation, which is a desirable measurement from the reliability perspective.

Wind Energ. 2016; **19**:1733–1747 © 2015 John Wiley & Sons, Ltd.
DOI: 10.1002/we

Table VI. PGB fault diagnostic results using individual CIs.

CI: FM0						
Classifier	KNN ($k = 15$)		BP ($N = 40$)		LAMSTAR	
Type of fault	Mean error (μ)	Std dev. (σ)	Mean error (μ)	Std dev. (σ)	Mean error (μ)	Std dev. (σ)
Healthy	24.56	2.94	47.79	20.27	62.97	7.95
Sun	39.48	3.04	47.08	26.97	73.11	6.70
Planet	38.66	3.24	51.04	21.41	66.65	10.87
Ring	49.03	2.89	43.33	31.43	78.25	6.49
Overall	37.94	1.31	47.24	12.38	70.24	1.56
CI: Res RMS						
Classifier	KNN ($k = 15$)		BP ($N = 30$)		LAMSTAR	
Type of fault						
Healthy	20.50	2.37	43.97	21.75	34.67	3.83
Sun	38.04	2.94	32.63	25.79	42.58	3.38
Planet	19.21	2.42	54.16	22.01	33.39	3.45
Ring	34.07	2.80	29.47	20.32	47.43	3.36
Overall	27.95	1.03	40.32	13.18	39.47	1.14
CI: GDF						
Classifier	KNN ($k = 15$)		BP ($N = 30$)		LAMSTAR	
Type of fault						
Healthy	12.30	2.01	24.30	11.80	12.7	1.98
Sun	25.11	2.59	45.45	32.60	28.12	2.94
Planet	22.14	2.39	31.81	12.96	26.13	2.62
Ring	15.13	1.85	15.89	15.70	16.01	1.65
Overall	18.67	0.87	29.64	12.86	20.74	1.07
CI: WEO RMS						
Classifier	KNN ($k = 15$)		BP ($N = 40$)		LAMSTAR	
Type of fault						
Healthy	77.20	2.28	62.37	25.16	73.50	7.72
Sun	70.79	2.47	73.67	12.83	78.67	6.76
Planet	73.65	2.39	80.26	13.13	77.91	8.06
Ring	70.24	2.23	84.54	12.87	75.27	7.08
Overall	72.97	1.03	75.20	12.29	76.34	0.95

Note: k is the search radius for a majority vote of its neighbors in KNN and N is the number of neurons in the hidden layer in BP network.

Table VII. PGB diagnostic results using CI combination.

First CI combination: FM0, Res RMS, WEO RMS, GDF						
Classifier	KNN ($k = 3$)		BP ($N = 40$)		LAMSTAR	
Type of fault	Mean error (μ)	Std dev. (σ)	Mean error (μ)	Std dev. (σ)	Mean error (μ)	Std dev. (σ)
Healthy	1.52	0.88	4.56	13.64	1.99	0.73
Sun	6.38	1.44	9.24	18.49	6.67	1.50
Planet	4.33	1.30	14.13	21.60	4.43	1.11
Ring	2.27	1.01	7.96	22.77	2.81	0.87
Overall	3.63	0.56	8.94	12.71	3.98	0.54
Second CI combination: P2P, FM0, Res RMS, Res KT, Res P2P, GDF, EO RMS, EO P2P, W RMS, W P2P, WEO RMS, WEO P2P, WEO KT, WEO SK.						
Classifier	KNN ($k = 4$)		BP ($N = 40$)		LAMSTAR	
Type of fault	Mean error (μ)	Std dev. (σ)	Mean error (μ)	Std dev. (σ)	Mean error (μ)	Std dev. (σ)
Healthy	28.73	2.47	14.33	18.19	29.15	2.67
Sun	23.11	2.65	22.42	22.76	22.29	2.38
Planet	21.24	2.38	14.06	13.03	19.31	2.00
Ring	29.73	2.68	11.44	18.02	30.04	2.40
Overall	25.71	1.20	15.51	12.44	25.20	1.22

Note: k is the search radius for KNN and N is the number of neurons in the hidden layer in BP network

5. CONCLUSION

In this paper, a new method using a single vibration sensor for PGB fault diagnosis was presented. It combines the techniques of enveloping, Welch's SA, and data mining-based fault classifiers. Using the presented approach, vibration fault features for wind turbine PGB are extracted as CIs and CIs are used as inputs to fault classifiers for PGB fault diagnosis. The presented method was validated with a set of seeded fault tests performed on a PGB test rig in a laboratory. First, the digitized accelerometer signals were processed by SA technique to extract PGB fault features and to compute CIs. The effective CIs were grouped into two combination sets according to the level of statistical separation followed by training three machine learning algorithms as fault classifiers: KNN, BP network, and LAMSTAR network. Each fault classifier was run 50 times to obtain the statistical results. The validation results have shown the following: (i) the minimal error rate of 3.63% was achieved using KNN when the first set of CI combination was used; (ii) an average diagnostic error rate of 8.94% was achieved using the BP algorithm. The local minima convergence was observed at a rate of 12 ~ 16% out of 50 runs. (3) LAMSTAR network displayed less sensitivity to the local minima issue and achieved a similar level of diagnostic error rate of 3.98% compared with KNN when the first set of CI combination was used. Also, LAMSTAR network resulted in the minimal standard deviation, which is a desirable measurement from the reliability perspective. In summary, the contribution of the paper is the development of a new method that combines techniques of enveloping, Welch's SA, and data mining-based fault classifiers for PGB fault diagnosis with a single vibration sensor. The developed method effectively differentiated the localized faults on all gears: sun gear, planetary gear, and ring gear, which has not been reported in the literature.

REFERENCES

1. Sheng S, Link H, LaCava W, van Dam J, McNiff B, Veers P, Keller J, Butterfield S, Oyague F. Wind turbine drivetrain condition monitoring during GRC phase 1 and phase 2 testing. NREL Technical Report: NREL/TP-5000-52748, National Renewable Energy Laboratory, Golden, CO, USA, 2011.
2. Sheng S. Gearbox reliability database: yesterday, today, and tomorrow, NREL Report No. PR-5000-63106 provided at the Wind Turbine Tribology Seminar, Argonne National Laboratory, Lemont, IL. Oct 29 – 31, 2014.
3. Braun S. The extraction of periodic waveforms by time domain averaging. *Acustica* 1975; **32**: 69–77.
4. McFadden PD. A revised model for the extraction of periodic waveforms by time domain averaging. *Mechanical Systems and Signal Processing* 1987; **1**: 83–95.
5. Samuel PD, Conroy JK, Pines DJ. Planetary transmission diagnostics. NASA Technical Report: NASA/CR-2004-213068, NASA Glenn Research Center, Cleveland, OH, 2004.
6. Luo H, Hatch C, Hanna J, Kalb M, Weiss A, Winterton J, Inalpolat M, Dannehy C. Amplitude modulations in planetary gears. *Wind Energy* 2014; **17**: 505–517. DOI: 10.1002/we.1545.
7. McFadden PD, Howard IM. The detection of seeded faults in an epicyclic gearbox by signal averaging of the vibration. Aeronautical Research Laboratory: Melbourne, Victoria, Australia, 1990.
8. Howard IM. Epicyclic transmission fault detection by vibration analysis. Australian Vibration and Noise Conference, Melbourne, Australia, 1990; 171–178.
9. McFadden PD. Window functions for the calculation of the time domain averages of the vibration of the individual planet gears and sun gear in an epicyclic gearbox. *Journal of Vibration and Acoustics* 1994; **116**: 179–187.
10. Lewicki DG, Laberge KE, Ehinger RT, Fetty J. Planetary gearbox fault detection using vibration separation technique, NASA Technical Report: NASA/CR-2004-213068, NASA Glenn Research Center, Cleveland, OH, 2011.
11. Kiddy JS, Samuel PD, Lewicki DG, LaBerge KE, Ehinger RT, Fetty J. Fiber optic strain sensor for planetary gear diagnostics. NASA Technical Report: NASA/TM-2011-217123, NASA Glenn Research Center, Cleveland, OH, 2011.
12. Yang W, Tavner PJ, Crabtree CJ, Feng Y, Qiu Y. Wind turbine condition monitoring: technical and commercial challenges. *Wind Energy* 2014; **17**: 673–693. DOI: 10.1002/we.1508.
13. Siegel D, Zhao W, Lapira E, AbuAli M, Lee J. A comparative study on vibration-based condition monitoring algorithms for wind turbine drive trains. *Wind Energy* 2014; **17**: 695–714. DOI: 10.1002/we.1585.
14. Luo H, Hatch C, Kalb M, Hanna J, Weiss A, Sheng S. Effective and accurate approaches for wind turbine gearbox condition monitoring. *Wind Energy* 2014; **17**: 715–728. DOI: 10.1002/we.1595.
15. Sawalhi N, Randall RB, Forrester D. Separation and enhancement of gear and bearing signals for the diagnosis of wind turbine transmission systems. *Wind Energy* 2014; **17**: 729–743. DOI: 10.1002/we.1671.

16. Wang J, Gao RX, Yan R. Integration of EEMD and ICA for wind turbine gearbox diagnosis. *Wind Energy* 2014; **17**: 757–773. DOI: 10.1002/we.1653.
17. Wu B, Saxena A, Khawaja TS, Patrick R, Vachtsevanos G, Sparis P. An approach to fault diagnosis of helicopter planetary gears. Proceedings of IEEE AUTOTESTCON, San Antonio, TX., 2004; 475–481.
18. Patrick R, Orchard ME, Zhang B, Koelemay MD. An integrated approach to helicopter planetary gear fault diagnosis and failure prognosis *Proceedings of IEEE AUTOTESTCON*, Baltimore, MD, 2007; 547–552.
19. Bartelmus W, Zimroz R. Vibration condition monitoring of planetary gearbox under varying external load. *Mechanical Systems and Signal Processing* 2009; **23**: 246–257.
20. Barszcza T, Randall RB. Application of spectral kurtosis for detection of a tooth crack in the planetary gear of a wind turbine. *Mechanical Systems and Signal Processing* 2009; **23**: 1352–1365.
21. Feng Z, Zuo MJ. Vibration signal models for fault diagnosis of planetary gearbox. *Journal of Sound and Vibration* 2012; **331**: 4919–4939.
22. Bechhoefer E, Van Hecke B, He D. Processing for improved spectral analysis. Proceedings of the Annual Conference of the Prognostics and Health Management Society, October 14 – 17, New Orleans, LA, 2013.
23. Van Hecke B, He D, Qu Y. On the use of spectral averaging of acoustic emission signals for bearing fault diagnostics. *ASME Journal of Vibration and Acoustics* 2014; **136**. DOI: 10.1115/1.4028322.
24. Welch P. The use of fast Fourier transform for the estimation of power spectra: a method based on time averaging over short, modified periodograms. *IEEE transactions on Audio Electroacoustics* 1967; **15**: 70–73.
25. Sheng S. Wind turbine gearbox condition monitoring round robin study – vibration analysis, NREL, Denver, CO, Tech. Rep. NREL/TP-5000-54530, Jul. 2012.
26. Harris CM. Harris' Shock and Vibration Handbook (5th edn). McGraw-Hill: New York, 2002.
27. Teager HM, Teager SM. Evidence for nonlinear sound production mechanisms in the vocal tract. In Speech Production and Speech Modeling Symposium, Time Frequency and Time-Scale Analysis, Hardcastle WJ Marchal A (eds.). Springer: Netherlands, 1992; **55**; 345–348.
28. Altman NS. An introduction to kernel and nearest-neighbor nonparametric regression. *The American Statistician* 1992; **46**: 175–185.
29. He D, Li R, Zhu J, Zade M. A data mining based full ceramic bearing fault diagnostic system using AE sensors. *IEEE Transactions on Neural Networks* 2011; **22**: 2022–2031.
30. Rumelhart DE, Hinton GE, Williams RJ. Learning representations by back-propagating errors. *Nature* 1986; **323**: 533–536.
31. Graupe D, Kordylewski H. A large memory storage and retrieval neural network for adaptive retrieval and diagnosis. *International Journal of Software Engineering and Knowledge Engineering* 1998; **8**: 115–138.
32. G Patent, [online] http://www.google.com/patents/US5920852, Oct 14, 2015.
33. Kohonen T. Self-Organization and Associative Memory. Springer-Verlag: Berlin, 1984.
34. Graupe D. Principles of Artificial Neural Networks (3rd edn). World Scientific Publishing Co.: Hackensack, NJ 07601, 2013.
35. Kordylewski H, Graupe D, Liu K. A novel large-memory neural network as an aid in medical diagnosis applications. *IEEE Transactions on Information Technology in Biomedicine* 2001; **5**: 202–209.
36. Bartelmus W, Zimroz R. Vibration spectra characteristic frequencies for condition monitoring of mining machinery compound and complex gearboxes. *Scientific Papers of the Institute of Mining, University of Technology, Studies and Research* 2011; **133**: 17–34.
37. Antoni J. Fast computation of the kurtogram for the detection of transient faults. *Mechanical Systems and Signal Processing* 2007; **32**: 108–124.